A Variational Approach to Shape from Defocus*

Hailin Jin and Paolo Favaro

Department of Electrical Engineering, Washington University, Saint Louis – MO 63130
Department of Computer Science, University of California, Los Angeles – CA 90095
{hljin,fava}@ee.wustl.edu

Abstract. We address the problem of estimating the three-dimensional shape and radiance of a surface in space from images obtained with different focal settings. We pose the problem as an infinite-dimensional optimization and seek for the global shape of the surface by numerically solving a partial differential equation (PDE). Our method has the advantage of being global (so that regularization can be imposed explicitly), efficient (we use level set methods to solve the PDE), and geometrically correct (we do not assume a shift-invariant imaging model, and therefore are not restricted to equifocal surfaces).

1 Introduction

Shape from defocus (SFD) consists of reconstructing the three-dimensional shape and radiance ("texture") of a scene from a number of images taken with different focal settings. It is one of the classical problems in Computer Vision. This problem can be posed as the inversion of certain integral equations that describe the imaging process. Once an optimality criterion has been chosen, the problem can then be solved uniquely under suitable conditions on the radiance and the shape of the scene [13].

What makes SFD possible is the fact that the image of a scene at a certain position on the image plane (a "pixel") depends upon the radiance on a region of the scene, as well as on the shape of such a region. What makes SFD possible, however, also makes it difficult: the image at a given pixel is obtained by integrating the (unknown) radiance of the scene against an (unknown) kernel that depends upon its shape. Given values of the integral at each pixel, one needs to estimate both the radiance and the kernel, which is known to be a severely ill-posed inverse problem in its full generality.

Several approaches have been presented to address this problem, which is an instance of "blind deblurring", or "blind deconvolution" if one is willing to make the simplifying assumption of shift-invariant kernels, as we describe in Section 1.1. Typically, the depth of the scene is computed after approximating (locally) the radiance of the scene using various classes of functions or filters.

In this paper, rather than estimating depth at each pixel, we formulate shape from defocus within a variational framework as the problem of estimating an infinite-dimensional surface in space. We derive the optimality conditions and design a numerical algorithm to efficiently reach a (local) minimum. We do not make the assumption that the imaging kernel is shift-invariant – one that is patently violated at occluding boundaries – and therefore we can easily handle complex shapes.

* This research is sponsored by ARO grant DAAD19-99-1-0139 and Intel grant 8029 to Stefano Soatto.

A. Heyden et al. (Eds.): ECCV 2002, LNCS 2351, pp. 18–30, 2002.

1.1 Relation to Previous Work

In the literature of computer vision, a number of algorithms have been proposed to estimate depth from defocus. The main assumption, common to most algorithms available in the literature, is that the scene is locally approximated by a plane parallel to the image plane [2,7,8,10,12,15,17,19,22,23,24,25,26]. This is called the *equifocal* assumption and it allows describing the imaging process as a linear convolution; the price to pay, however, is a fundamental trade-off between robustness and precision. In order to increase the reliability of the estimation, one would want to integrate over regions that are as large as possible; on the other hand, for the equifocal assumption to be valid, one would want regions to be as small as possible. In particular, at occluding boundaries the equifocal assumption is violated altogether.

Several algorithms have been also proposed to solve the problem in the shift-variant case as, for example, in [18]. [4] presents several methods for this purpose. The *block-variant blur* methods correct the assumption of local equifocal imaging by taking into account contributions from the neighboring regions. Other techniques are the complex spectrogram and the Wigner distributions, which are applied in a *space-frequency* framework. A successful approach employs a *Markov random field* model to obtain a *maximum a-posteriori* estimate of the blurring parameters.

1.2 Main Contributions

The equifocal assumption impacts both the shape reconstruction and radiance restoration.

Shape estimation is affected by how well an equifocal plane approximates (locally) the observed surface. This, in particular, implies that, within the surface, the best candidates will have equifocal tangent planes. It is clear that, unless the whole surface is close to be a plane parallel to the image plane, these candidates will be isolated points or curves. This implies that, in general, the estimation will be incorrect almost everywhere. Also, notice that this behavior does not depend on the smoothness of the surface. For example, if we consider a slanted plane, which is a smooth surface, any algorithm relying on the assumption above will result in a biased shape estimation.

Since the equifocal assumption at a point holds in general only locally, it is always associated with the choice of a domain around that point. Typically, such a domain is a square window. This is also the domain where the radiance is reconstructed. Notice, however, that when the chosen window is not in focus, it will receive contributions from the radiance lying on the neighboring regions, which are not accounted for in the imaging model. This implies that, regardless of the information carried by the texture of the radiance, the restoration of regions with higher intensity gradient (energy) will be favored over that of regions with lower intensity gradient.

These limitations motivate us to take a different approach. In this paper we forgo the equifocal assumption by approximating the scene with tangent planes, so that we can integrate visual information over the entire image. This results in superior resistance to noise (as also noticed in [4]). We formulate the problem within a variational framework, so that we can regularize the reconstruction process via imposing smoothness, and we do not make explicit approximations of the shape; rather, we estimate shape via

optimization on the infinite-dimensional space of smooth surfaces. We compute the necessary optimality conditions and numerically implement a partial differential equation to converge to a (local) minimum. Last, but not least, we achieve superior computational efficiency by estimating global shape, as opposed to depth at each pixel since the radiance on overlapping regions does not need to be recomputed.

2 Optimal Shape from Defocus

Let P be a generic point on the surface s in the scene with coordinates $\mathbf{X} \in \mathbb{R}^3$. Suppose that we are imaging the scene using a real aperture optical system with focal setting η. By exploiting the additive nature of the energy transport phenomena, we model the image formation process with an integral of the form

$$I_\eta(\mathbf{x}) = \int_s h_\eta(\mathbf{X}, \tilde{\mathbf{X}}) r(\tilde{\mathbf{X}}) dA(\tilde{\mathbf{X}}) \tag{1}$$

where $\mathbf{x} = \pi_\eta(\mathbf{X}) \in \mathbb{R}^2$ is the projection of P on the image plane, which depends on the geometry of the optics, and in particular on the focal setting η, and $dA(\tilde{\mathbf{X}})$ is the Euclidean area form of s at $\tilde{\mathbf{X}}$. r is the *radiance density* of the scene and h_η is the imaging kernel, which depends on the geometry of the imaging device. h_η satisfies the normalization constraint, i.e. for any surface s

$$\int_s h_\eta(\mathbf{X}, \tilde{\mathbf{X}}) dA(\tilde{\mathbf{X}}) = 1. \tag{2}$$

We are able to measure the intensity $I(\mathbf{x})$ at each point $\mathbf{x}$. Our goal is to reconstruct both the radiance r and the shape s of the scene from a collection of images obtained with different focal settings.

Suppose we have L images with different settings $\eta_1, \ldots, \eta_L$. We collect and organize these images into an array $I \doteq [I_{\eta_1}, \ldots, I_{\eta_L}]^T$, and do the same for the respective kernels $h \doteq [h_{\eta_1}, \ldots, h_{\eta_L}]^T$. The right-hand side of equation (1) can also be interpreted as the *synthetic image* generated by a given surface s radiating energy with a given radiance density r. In this case we denote the collection of all such images with $J \doteq [J_{\eta_1}, \ldots, J_{\eta_L}]^T$.

2.1 Cost Functional

Inverting the integral in equation (1) based on measurements I is an ill-posed problem. Furthermore, often (1) is only an approximation of the model that generates the data. We will therefore look for solutions that minimize a suitable *optimization criterion*. In [6] Csiszár presents a derivation of "sensible" optimization criteria for the problem above, and concludes that the only two that satisfy a set of consistency axioms are the L_2-norm – when the quantities at play are unconstrained – and the information-divergence – when both the radiance and the kernel are constrained to be non-negative. The latter criterion applies to our case since the radiance represents an energy density and the kernel

represents surface area. Therefore, without further discussion, we adopt the information-divergence (or I-divergence) as a cost functional for the discrepancy between measured images I and the synthetic images J:

$$\Psi(I|J) = \int_s \Phi(I(\mathbf{x})|J(\mathbf{x}))dA \tag{3}$$

where

$$\Phi(I(\mathbf{x})|J(\mathbf{x})) = I(\mathbf{x}) \log \frac{I(\mathbf{x})}{J(\mathbf{x})} - I(\mathbf{x}) + J(\mathbf{x}) \tag{4}$$

$\mathbf{x} = \pi(\mathbf{X})$, $\mathbf{X}$ belongs to the shape s. Notice that our cost functional (3) is defined for the surface s, instead of the image domain as commonly seen in the literature. This allows us to derive a geometric flow (see Section 2.2) to minimize the cost functional with respect to the surface. To emphasize the dependency of J on the surface s and the radiance r, we write, with an abuse of notation, $J = J(s, r)$.

Hence, the problem of retrieving both shape s and radiance r from a collection of images $I \doteq [I_{u_1}, \ldots, I_{u_L}]^T$ can be formulated as that of finding a minimizer $(\hat{s}, \hat{r})$ for the I-divergence between I and $J = J(s, r)$:

$$(\hat{s}, \hat{r}) = \arg\min_{(s,r)} \Psi\big(I|J(s, r)\big). \tag{5}$$

2.2 Radiance and Shape Estimation

The problem of minimizing the cost functional (3) involves solving a nonlinear optimization problem for two unknowns, which are both infinite-dimensional. To our best knowledge, there is no direct solution to minimize simultaneously both the shape s and radiance r, so we choose to divide the optimization into two sub-problems through an *alternating minimization* technique. Suppose we are given an initial guess for the radiance r_0 and the surface s_0 (see Section 3.4 for more details on initialization), then the algorithm can be written as:

$$\begin{cases} \hat{r}_{k+1} = \arg\min_r \Psi(I|J(\hat{s}_k, r)) \\ \hat{s}_{k+1} = \arg\min_s \Psi(I|J(s, \hat{r}_{k+1})). \end{cases} \tag{6}$$

The enabling step to use such an alternating minimization relies on having two iterations that independently lower the value of the cost functional, so that their combination leads toward the (local) minimum. For the first part we employ an iterative formula on the radiance r, which is constrained to be strictly positive, obtained from the Kuhn-Tucker conditions [11] on the cost functional. For the second part we use a gradient descent flow implemented using level set methods [16].

Radiance Iteration. Any radiance r that minimizes the cost function must satisfy the following necessary conditions:

$$\int_s \frac{h(\mathbf{X}, \tilde{\mathbf{X}}) I(\pi(\mathbf{X}))}{\int_s h(\mathbf{X}, \tilde{\mathbf{X}}) r(\tilde{\mathbf{X}}) dA(\tilde{\mathbf{X}})} dA(\mathbf{X}) \begin{cases} = \int_s h(\mathbf{X}, \tilde{\mathbf{X}}) dA(\mathbf{X}) & \forall\, \tilde{\mathbf{X}} : r(\tilde{\mathbf{X}}) > 0 \\ \leq \int_s h(\mathbf{X}, \tilde{\mathbf{X}}) dA(\mathbf{X}) & \forall\, \tilde{\mathbf{X}} : r(\tilde{\mathbf{X}}) = 0 \end{cases} \tag{7}$$

These are the Kuhn-Tucker conditions, and since no closed-form solution is generally available, we seek for an iterative procedure such that the radiance will converge to a fixed point. Following Snyder et al. [21] we define the iteration as:

$$\hat{r}_{k+1}(\tilde{\mathbf{X}}) = \hat{r}_k(\tilde{\mathbf{X}}) \frac{1}{\int_s h(\mathbf{X}, \tilde{\mathbf{X}}) dA(\mathbf{X})} \int_s \frac{h(\mathbf{X}, \tilde{\mathbf{X}}) I(\pi(\mathbf{X}))}{\int_s h(\mathbf{X}, \bar{\mathbf{X}}) \hat{r}_k(\bar{\mathbf{X}}) dA(\bar{\mathbf{X}})} dA(\mathbf{X}). \quad (8)$$

It can be shown that this iteration provably minimizes the chosen cost functional (with respect to r) even when the iteration is computed without the correct shape s [10].

Gradient Descent Flow We minimize (3) with respect to the surface s by introducing an auxiliary time variable t and deforming the surface $s(t) \doteq \{P(\mathbf{X}, t) : \mathbf{X} \in s\}$ in time t starting from an initial surface $s(0)$. The evolution is governed by a partial differential equation:

$$P_t = \mathcal{EL}(\mathbf{X}, s) N, \quad (9)$$

where N is the unit normal to the surface at P and $\mathcal{EL}(\mathbf{X}, s) = 0$ is the Euler-Lagrange equation of the cost function (3). Note that in equation (9) we let the surface deform only along the normal direction, because the deforming in the tangent space will not change the shape of the surface (what it changes is the parameterization). This PDE is the *gradient descent flow*. When this flow converges to the steady state, i.e. $P_t = 0$, the Euler-Lagrange equation is satisfied. And it can also be shown that the cost functional monotonically decreases with respect to t (if a suitable initial shape $P(\mathbf{X}, 0)$ is provided). Therefore, we are guaranteed to reach a (local) minimum of the cost function.

Away from discontinuities, we approximate the surface locally around $P(\mathbf{X}, t)$ with the tangent plane T_P. Note that this approximation is fundamentally different from the equifocal assumption, because the tangent plane is not necessarily parallel to the focal plane. Hence the resulting kernel h is not shift-invariant. We assume that the radiance r is defined on a neighborhood around s (see Section 3.3 for more details on how to extend the radiance into $\mathbb{R}^3$). A point $\mathbf{Y}$ in T_P satisfies the identity $N^T \mathbf{Y} = N^T \mathbf{X}$, where N is the unit normal vector of s at P. Let K be the transformation bringing local coordinates (u, v) to points in T_P, $K : \Omega \subset \mathbb{R}^2 \to T_P$. K can always be assumed to take the following form as long as the third component of N is non-zero:

$$\mathbf{Y} = K(\mathbf{X}, u, v) = \mathbf{X} + [\, u \; v \; k(u, v) \,]^T. \quad (10)$$

Immediately we have

$$k(u, v) = -\frac{N_1 u + N_2 v}{N_3}, \quad (11)$$

where N_1, N_2 and N_3 are the components of N. Hence K explicitly depends on $\mathbf{X}$ and N. Under these assumptions, the model image J can be computed as:

$$J(\pi(\mathbf{X})) = \int h\left(\mathbf{X}, \mathbf{X} + K\left(u, v\right)\right) r\left(\mathbf{X} + K\left(u, v\right)\right) du dv. \quad (12)$$

In [9], Faugeras and Keriven prove that the Euler-Lagrange equation for (3) takes the following form:

$$\mathcal{EL}(\mathbf{X}, s) = H\Phi - \Phi_{\mathbf{X}} \cdot N - H(\Phi_N \cdot N) + \mathrm{Tr}\left((\Phi_{\mathbf{X}N})_{T_P} + dN \circ (\Phi_{NN})_{T_P} \right) = 0 \quad (13)$$

where $Tr(\cdot)$ denotes the trace; H is the mean curvature, and $\Phi_{\mathbf{X}}$ and Φ_N stand for the derivatives of Φ with respect to $\mathbf{X}$ and N respectively. Φ_{NN} and $\Phi_{\mathbf{X}N}$ are the second order derivatives of Φ and $(\Phi_{NN})_{T_P}$ and $(\Phi_{\mathbf{X}N})_{T_P}$ are their restrictions to the tangent plane T_P. dN is the differential of the Gauss map of the surface, which involves the second fundamental form. Writing the expressions explicitly, we have:

$$\begin{aligned}
\Phi_{\mathbf{X}} &= \log\left(\frac{I}{J}\right) I_{\mathbf{X}} + \left(1 - \frac{I}{J}\right) J_{\mathbf{X}} \\
\Phi_N &= \left(1 - \frac{I}{J}\right) J_N \\
I_{\mathbf{X}} &= \nabla I \cdot \frac{\partial \pi(\mathbf{X})}{\partial \mathbf{X}} \\
J_{\mathbf{X}} &= \int \left(h_{\mathbf{X}} r + h \nabla r\right) du dv \\
J_N &= \int \frac{\partial K}{\partial N} \left(h_{\mathbf{X}} r + h \nabla r\right) du dv
\end{aligned}$$

Note that we have skipped the arguments of all the functions for ease of notation. Similarly we can compute $\Phi_{\mathbf{X}N}$ and Φ_{NN}.

Finally, the gradient descent flow of $P(\mathbf{X}, t)$ is:

$$P_t = \left(H\Phi - \Phi_{\mathbf{X}} \cdot N - H(\Phi_N \cdot N) + \mathrm{Tr}\left((\Phi_{\mathbf{X}N})_{T_P} + dN \circ (\Phi_{NN})_{T_P}\right)\right) N. \quad (14)$$

Since the flow (14) depends only on the first and second derivatives of Φ with respect to $\mathbf{X}$ and N and geometric quantities, namely, H, N, dN, T_P, the flow is independent of any particular parameterization of the surface one chooses. In this sense, the flow is intrinsic. Experimentally, we find that the following first-order approximation of the flow (14) yields very similar results to those of the full second-order flow, while avoiding the time-consuming computation of $\Phi_{\mathbf{X}N}$ and Φ_{NN}:

$$P_t = \left(H\Phi - \Phi_{\mathbf{X}} \cdot N - H(\Phi_N \cdot N)\right) N. \quad (15)$$

3 Implementation

3.1 Level Set Iteration

We implement the flow (14) and (15) using level set methods. The level set methods were originally developed by Osher and Sethian [16]. Since then, the methods have gained popularity in various fields. Many fast numerical schemes have been proposed based on it. For a complete account refer to [20]. The level set implementation of any geometric flow begins by embedding the initial interface $P(\mathbf{X}, 0)$ as a level set of a scalar function $\psi_0(\mathbf{X})$ which is then taken to be the initial condition for a function over time $\psi(\mathbf{X}, t)$:

$$\psi_0 : \mathbb{R}^3 \to \mathbb{R}, \quad \psi : \mathbb{R}^3 \times \mathbb{R}^+ \to \mathbb{R}, \quad \psi(\mathbf{X}, 0) = \psi_0(\mathbf{X}).$$

The choice of a particular level set is arbitrary but is typically taken to be zero. The key point is that the interface is continuously embedded within the same fixed level set of ψ

at all times. Thus, choosing the zero level set we have

$$\psi_0(P(\mathbf{X},0)) = 0, \quad \text{and} \quad \psi(P(\mathbf{X},t),t) = 0.$$

Differentiating with respect to t therefore yields:

$$\psi_t + \nabla\psi \cdot P_t = 0 \tag{16}$$

an evolution equation for ψ (where $\nabla\psi = \psi_{\mathbf{X}}$) which evolves the interface $P(\mathbf{X},t)$ described implicitly by $\psi(\mathbf{X},t) = 0$ for all t.

3.2 Intersection with the Surface

In the radiance iteration it is necessary to determine which point on the surface s corresponds to which point on the image plane, in order to establish the blurring radius of the kernel h. To be more specific, one needs to compute the intersection of a ray, which depends on the imaging model, with the surface s. Obtaining explicitly all the possible intersections with a discrete representation of the surface, for instance a triangulated mesh, turns out to be a computationally expensive task. Rather, it is possible to do this very efficiently by exploiting the advantage of an implicit formulation of the shape, i.e. the level set function ψ or the signed distance function. Let the ray be defined by a point X_0 and a direction v. Let X be the intersection we are looking for. X satisfies the following (nonlinear) ordinary differential equation:

$$\begin{cases} \frac{dX}{dt} & = c(X) \cdot v \\ X(0) & = X_0 \end{cases} \tag{17}$$

where $c(\cdot)$ is a scalar speed function defined as follows

$$c(X) = \begin{cases} \text{sign}(\psi(X)) & \text{if } |\psi(X)| > 1 \\ \psi(X) & \text{if } |\psi(X)| \leq 1 \end{cases}. \tag{18}$$

The rationale is that we move X according to $c(\cdot)$ so that X is lead towards the surface. When X crosses the surface, $c(X)$ will change sign accordingly, and therefore X will be forced to move in the opposite direction. Hence, X will oscillate around the intersection of the ray with the surface, reducing the overshoot at each step. Finally, we decide for X to be the intersection when the oscillation remains within a fixed band around the surface. This happens typically within a few iterations (3 to 5).

3.3 Radiance Extension

As mentioned in Section 2.2, we assume that the radiance is defined in a neighborhood around the surface s. Since the radiance is originally defined only on the surface (or the zero level set of ψ), we need to find a way to extend it. One way to do so, which is widely used in the literature of applied mathematics [5,27], is to extend r such that it is constant along the normals of s. This means that the extension should satisfy

$$\nabla r \cdot \nabla\psi = 0. \tag{19}$$

To solve the above equation we numerically search for the steady state solution of the following PDE:

$$\frac{\partial r}{\partial t} + \text{sign}(\psi)(\nabla r \cdot \nabla \psi) = 0. \tag{20}$$

Note that this keeps r on the zero level set of ψ (the surface s) unchanged. However, as a result of this process, the data is now defined in a neighborhood of s. The equation (20) can be efficiently solved using the fast marching technique [20].

3.4 Initialization

To start the alternating minimization one needs to have an initial guess for both radiance and surface. Since we have no prior knowledge on either unknown, we proceed as follows: choose one of the input images I_{u_1}, taken with focal setting u_1; define the initial surface as a plane parallel to the focal plane passing through the focal depth u_1; compute the radiance by back-projecting the image I_{u_1} onto the defined surface. As we see in our experiments, such a choice is not crucial to the estimation process. However, we also notice that a good initialization speeds up the minimization procedure considerably. Therefore, during the first steps of our algorithm we perform the surface estimation using a simple search of the minimum of the cost functional computed over a small grid of possible depths, assuming the surface is locally a plane. This initial surface is then used for the radiance iteration step after being smoothed. Later we substitute the search step with the level set iteration and proceed with the minimization as described in the previous sections.

4 Experiments

In this section we report some experiments with real images. Figure 1 shows two images which are obtained by changing the position of the image plane along the optical axis, and keeping the lens position fixed with respect to the scene. Moving the image plane necessarily involves scaling the images, which we avoid by employing a telecentric optical model (see [14]) and registering the two images using auxiliary patterns. Images are taken with an 8-bit camera containing two independently moving CCDs (kindly made available to us by S. K. Nayar). The near and far focused images in Figure 1 have focal depths of approximately $0.9m$ and $1.1m$ respectively. The focal length is $35mm$ and the lens aperture is $F/8$. The scene has been chosen so as to test the performance of the proposed algorithm when the usual equifocal assumption does not hold. It can be noticed that the scene presents significant depth variations and several occluding boundaries. In particular, at the occluding boundaries of the statues and in the folds of the skirts, the planar approximation fails. Furthermore, the blurring radii are up to $4-5$ pixels, so that the window size would have to be at least of 10 pixels, which would not allow for fine depth retrieval. In Figure 2 we show the corresponding surface evolution from the level set iteration. Figure 3 shows three steps of the radiance iteration during the alternating minimization procedure. Then, in Figure 4 we show the final estimate of the shape coded in gray level (256 values), where darker means closer to the viewer and brighter means farther from the viewer. Three views of the final shape which has been texture-mapped with the final radiance are also shown.

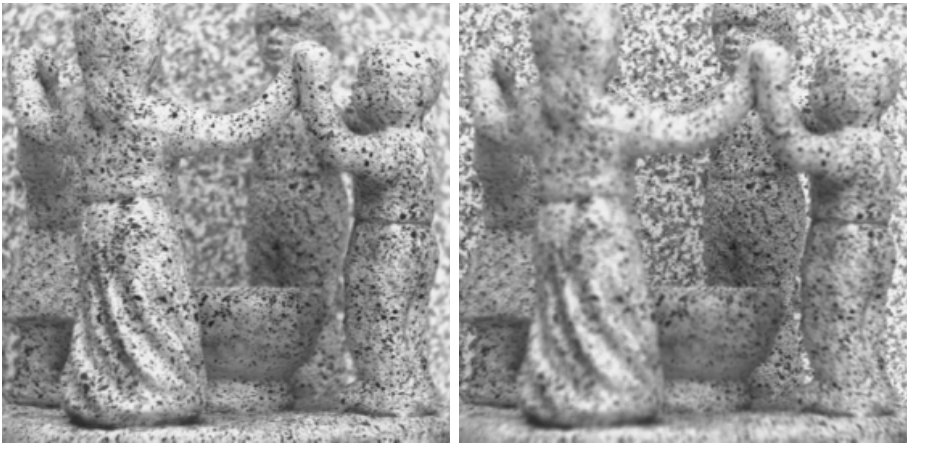

Fig. 1. Original images: *the left image is near-focused (*$0.9m$*). The right image is far-focused (*$1.1m$*). As it can be noticed, in both images the blurring is quite large, the shape is non-trivial and presents several discontinuities due to occluding boundaries. The blurring radii for both images are about 3-4 pixels.*

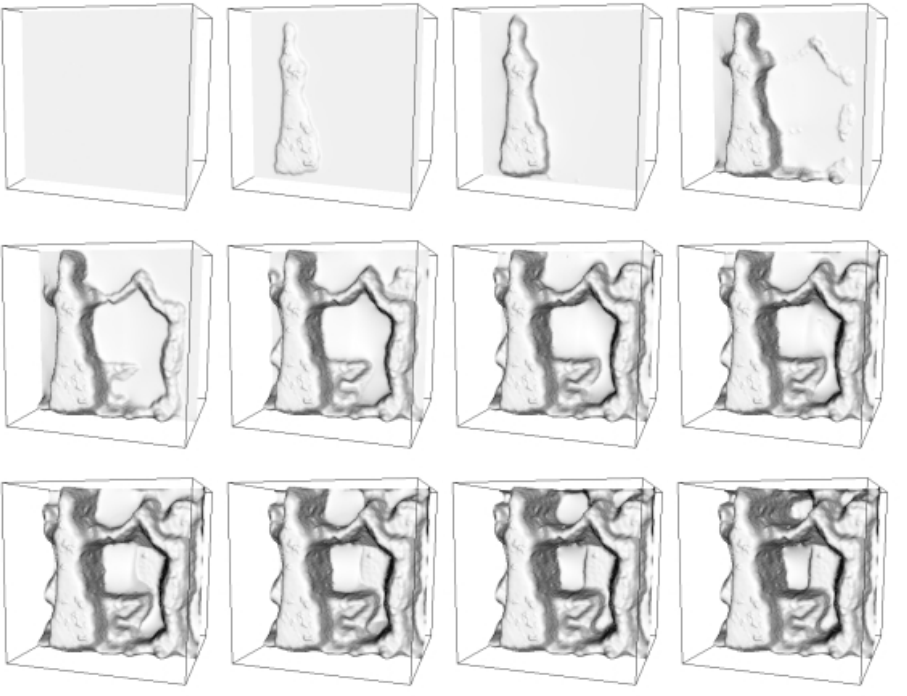

Fig. 2. Shape evolution:*Twelve snapshots of the shape evolution: the surface is gradually converging to the final shape, starting from a plane placed at depth* $0.9m$*.*

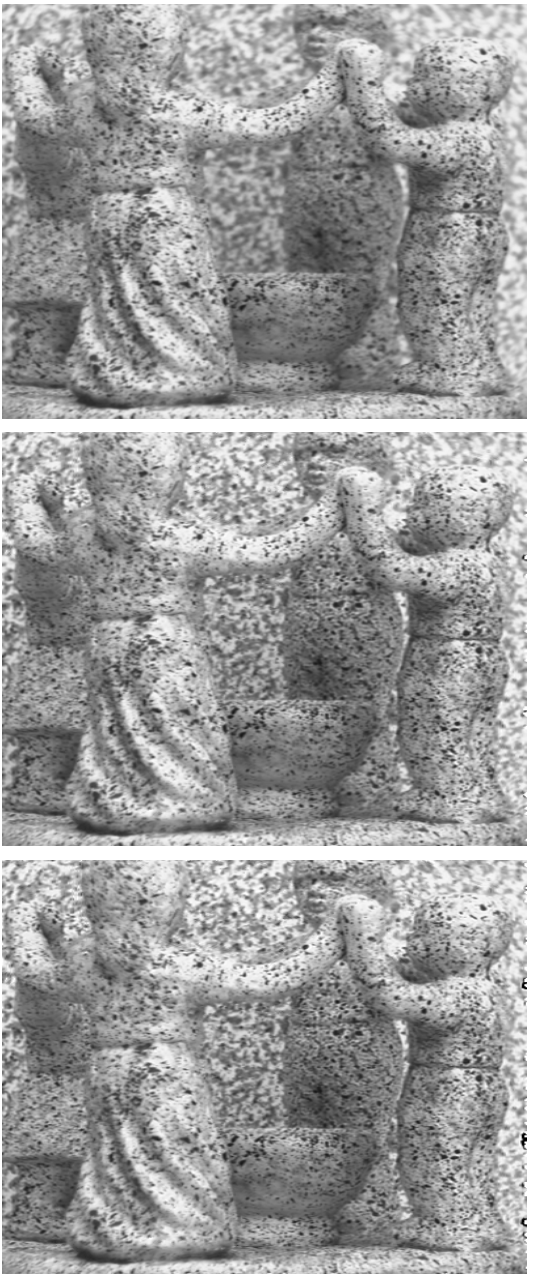

Fig. 3. *Three snapshots from the radiance iteration.* **Top***: Initial radiance obtained from the near focused image;* **Middle***: Radiance obtained after one iteration;* **Bottom***: Radiance after three steps. It can be noticed that the radiance is gradually sharpening after each iteration, as is particularly visible in the background. The final radiance is sharp everywhere.*

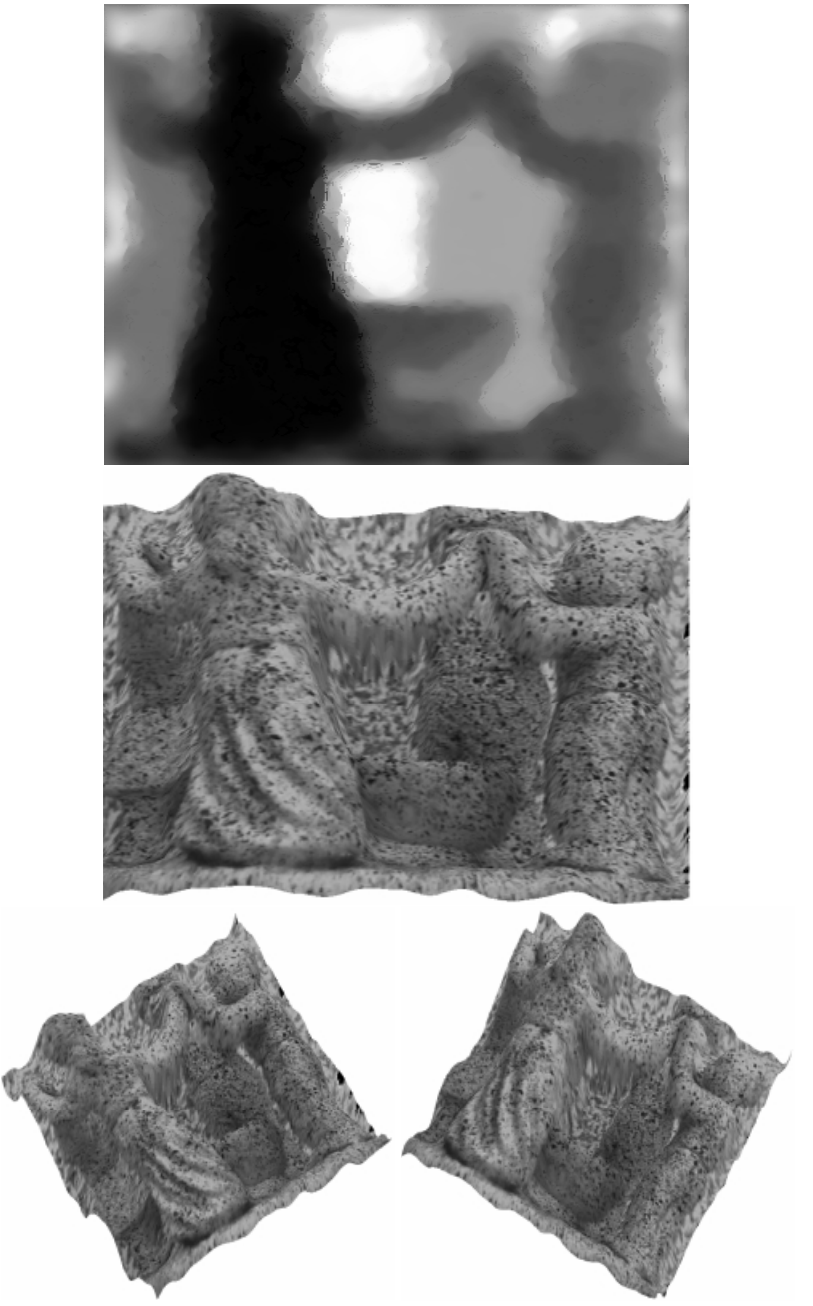

Fig. 4. Top: *depth rendered in gray levels (*256 *values) where darker means closer to the viewer and brighter means farther from the viewer;* **middle, bottom-left and bottom-right :** *three views of the final estimated shape, texture-mapped using the final estimated radiance.*

5 Conclusion

In estimating shape from defocus, the equifocal assumption is a well-known limitation. It introduces several disruptions in the reconstruction process such as image overlapping, windowing effects, edge bleeding, etc. We present a novel approach to shape from defocus based on an alternating minimization algorithm which does not make use of the equifocal assumption so as to overcome the above limitations. The radiance of the scene is estimated through an iterative scheme which provably converges to a minimum, while the shape is estimated using a gradient descent flow, which is then implemented numerically using level set methods. We show that the combination of these two steps leads to a (local) minimum of the discrepancy between the measured image and the modeled image. Also, by implementing the shape estimation with level set methods, we implicitly impose smoothness on the estimated shape in a completely automatic fashion.

Acknowledgements. The authors wish to thank Stefano Soatto and Anthony J. Yezzi for their helpful suggestions and invaluable support.

References

1. Special issue on blind system identification and estimation. *Proceedings of the IEEE*, October 1998.
2. N. Asada, H. Fujiwara, and T. Matsuyama. Edge and depth from focus. *Intl. J. of Comp. Vision*, 26(2):153–163, 1998.
3. W. Boothby. *Introduction to Differentiable Manifolds and Riemannian Geometry*. Academic Press, 1986.
4. S. Chaudhuri and A. Rajagopalan. *Depth from defocus: a real aperture imaging approach.* Springer Verlag, 1999.
5. S. Chen, B. Merriman, S. Osher and P. Smereka. A simple level set method for solving Stefan problems. *Journal of Computational Physics*, 135, 1995.
6. I. Csiszár. Why least-squares and maximum entropy; an axiomatic approach to inverse problems. *Annals of statistics*, 19:2033–2066, 1991.
7. T. Darell and K. Wohn. Depth from focus using a pyramid architecture. *Pattern Recognition Letters*, 11(2):787–796, 1990.
8. J. Ens and P. Lawrence. An investigation of methods for determining depth from focus. *IEEE Trans. Pattern Anal. Mach. Intell.*, 15:97–108, 1993.
9. O. Faugeras and R. Keriven. Variational principles, surface evolution pdes, level set methods and the stereo problem. *INRIA Technical report*, 3021:1–37, 1996.
10. P. Favaro and S. Soatto. Shape and reflectance estimation from the information divergence of blurred images. In *European Conference on Computer Vision*, pages 755–768, June 2000.
11. D. Luenberger. *Optimization by vector space methods*. Wiley, 1968.
12. J. Marshall, C. Burbeck, and D. Ariely. Occlusion edge blur: a cue to relative visual depth. *Intl. J. Opt. Soc. Am. A*, 13:681–688, 1996.
13. A. Mennucci and S. Soatto. On observing shape from defocused images. In *Proc. of the Intl. Conf. on Image Analysis and Processing*, pages 550–555, 1999.
14. M. Watanabe and S. K. Nayar. Telecentric optics for constant magnification imaging. In *Technical Report CUCS-026-95*, pages Dept. of Computer Science, Columbia University, New York, USA, 1995.

15. S. K. Nayar and Y. Nakagawa. Shape from focus. *IEEE Trans. Pattern Anal. Mach. Intell.*, 16(8):824–831, 1994.
16. S. Osher and J. A. Sethian. Fronts propagating with curvature-dependent speed: algorithms based on hamilton-jacobi equations. *J. of Comp. Physics*, 79:12–49, 1988.
17. A. Pentland. A new sense for depth of field. *IEEE Trans. Pattern Anal. Mach. Intell.*, 9:523–531, 1987.
18. A. N. Rajagopalan and S. Chaudhuri. A variational approach to recovering depth from defocused images. *IEEE Transactions on Pattern Analysis and Machine Intelligence*, 19(10):1158–64, October 1997.
19. Y. Schechner and N. Kiryati. The optimal axial interval in estimating depth from defocus. In *Proc. of the Intl. Conf. of Comp. Vision*, pages 843–848, 1993.
20. J. A. Sethian. *Level Set Methods: Evolving Interfaces in Geometry, Fluid Mechanics, Computer Vision, and Material Science*. Cambridge University Press, 1996.
21. D. L. Snyder, T. Schulz, and J. A. O'Sullivan. Deblurring subject to nonnegativity constraints. *IEEE Trans. on Signal Processing*, 40(5):1143–1150, 1992.
22. S. Soatto and P. Favaro. A geometric approach to blind deconvolution with application to shape from defocus. In *Intl. Conf. on Computer Vision and Pattern Recognition*, pages 10–17, June 2000.
23. M. Subbarao and G. Surya. Depth from defocus: a spatial domain approach. *Intl. J. of Computer Vision*, 13:271–294, 1994.
24. M. Watanabe and S. K. Nayar. Rational filters for passive depth from defocus. *Intl. J. of Comp. Vision*, 27(3):203–225, 1998.
25. Y. Xiong and S. Shafer. Depth from focusing and defocusing. In *Proc. of the Intl. Conf. of Comp. Vision and Pat. Recogn.*, pages 68–73, 1993.
26. D. Ziou. Passive depth from defocus using a spatial domain approach. In *Proc. of the Intl. Conf. of Computer Vision*, pages 799–804, 1998.
27. H. K. Zhao, T. Chen, and B. Merriman, and S. Osher. A variational level set approach to multiphase motion. *Journal of Computational Physics* 127, pages 179–195, 1996.